Starch - Stärke

WILEY-VCH

Starch

RESEARCH ARTICLE OPEN ACCESS

Effect of Infrared Heat-Moisture Treatment and Cooling Rate on the Material Properties of Amylose–Lipid Complex Nanomaterials

Njabulo Gideon Maphumulo[1] | Mondli Abednicko Masanabo[1] | Suprakas Sinha Ray[1,2] | Mohammad Naushad Emmambux[1]

[1]Department of Consumer and Food Sciences, Faculty of Natural and Agricultural Sciences, University of Pretoria, Hatfield, South Africa | [2]Centre for Nanostructures and Advanced Materials, DSI-CSIR Nanotechnology Innovation Centre, Council for Scientific and Industrial Research, Pretoria, South Africa

Correspondence: Mohammad Naushad Emmambux (Naushad.emmambux@up.ac.za)

Received: 20 January 2025 | **Revised:** 19 May 2025 | **Accepted:** 4 June 2025

Funding: This study was funded by the DSI/NRF Centre of Excellence in Food Security Grant ID number 91490 and University of Pretoria research support.

Keywords: cooling | crystallinity | flow properties | maize starch | V-amylose

ABSTRACT

There are limited food-compatible nanomaterials to be used in foods, or most of them are not considered as edible or clean label. Isolated amylose–lipid complex (ALC) nanomaterials were subject to infrared heat moisture treatment (IR-HMT) at 110°C for 1, 2, and 3 h continuously or IR-HMT for 1 h followed by different cooling systems (room temperature, refrigeration temperature, and liquid nitrogen) and repeated two more times. Differential scanning calorimetry (DSC) revealed that IR-HMT and an increase in cooling rates resulted in ALC nanomaterials with higher endothermic peak temperatures (T_p) (109–112°C) and the presence of Type II crystallites. Notably, IR-HMT and cooling with room temperature resulted in Type IIa ALC (T_p = 109°C), while cooling with refrigeration temperatures and liquid nitrogen resulted in Type IIb ALC nanomaterials (110–112°C). X-ray diffraction (XRD) revealed higher crystallinity (up to 21%) for IR-HMT ALC with different cooling systems compared to their untreated counterparts (13%). Furthermore, faster cooling resulted in ALC nanomaterials with higher crystallinity compared to slower cooling rate. IR-HMT resulted in ALC nanomaterials with lower viscosity compared to untreated ALC as observed from flow properties. Furthermore, they displayed lower water absorption and solubility indices, suggesting that IR-HMT and different cooling systems led to molecular changes in ALC nanomaterials that affected their properties.

1 | Introduction

Nanomaterials are generally defined as materials with one or more dimensions on a scale range of 1–100 nm. The use of nanomaterials in food processing and packaging has been gaining popularity over the past decades, owing to their nanoscale size [1]. The nanoscale size range results in materials that exhibit physical and chemical properties that are significantly different from the properties of macroscale materials composed of the same substances [2]. However, there are limited nanomaterials that are compatible for use in foods and edible packaging. Moreover, most of them are not considered as edible or "clean label". Recent consumer trends toward "clean label" food ingredients and foods have prompted research toward the development of nanomaterials suitable for use in food or are "clean label" [3, 4].

In recent years, clean label amylose–lipid complex (ALC) nanomaterials have been isolated [3] and patented US

Abbreviations: IR-HMT, infrared heat moisture treatment; T_g, glass transition temperature.

20200305455 A1 [5]. These ALCs have been produced by wet heat processing of starch with stearic acid for a prolonged period of time (up to 130 min) at 91°C, followed by hydrolysis of the amorphous components using thermostable alpha amylase to isolate the ACL nanomaterials [3]. The ALC nanomaterials isolated from maize starch and stearic acid, also known as V-ALCs have been reported to be round/ovoid flattened shape with an average particle size of 5.2–31.6 and 2.4–6.7 nm based on AFM and HRTEM, respectively [3]. ALC nanomaterials, isolated through complexation of amylose and *n*-butanol followed by alpha amylase hydrolysis, were also reported to be ovoid/circular to irregular in shape and had an average diameter of 10–20 nm [6].

Heat moisture treatment (HMT) is a physical method that has been used to modify the properties of starch, such as thermal, crystallinity, and pasting properties [7, 8]. It generally involves heating of the starch with reduced moisture content (10%–30%), below the gelatinization temperature (90–120), but above the glass transition temperature (T_g) for an extended time (0.25–16 h) [9, 10]. HMT of starch has been shown to enhance the crystalline nature of starch by increasing the interactions between amylose and amylopectin side chains, hence strengthening the intramolecular hydrogen bonds [9, 11]. Therefore, it can be suggested that HMT can be used to modify the properties of ALC nanomaterials by promoting stronger interactions, thus altering the crystallinity, thermal, and functional properties. However, HMT of starch has been criticized, since it takes long hours (up to 16 h), thus an energy-intensity method [12].

Infrared heat moisture treatment (IR-HMT) has been suggested to be a convenient, less time-consuming, and energy-efficient alternative to conventional HMT to modify starch [13, 14]. This technique has been shown to increase the amylose and amylopectin mobility, promotes hydrogen bonding and amylose–amylose reassociations, leading to starch with higher crystallinity [13]. Therefore, it can be hypothesized that IR-HMT could alter the properties of ALC nanomaterials, resulting in higher crystallinity for potential use as a filler in nanocomposite materials. However, repeated HMT has been previously shown to be more effective in altering the properties of starch compared to continuous HMT [15, 16].

Cooling rate after heating starch-based materials above glass transition (T_g) has been shown to affect the properties of the resulting materials. Wang et al. [17] investigated the effect of cooling temperature (20, 5, −10, and −20°C) on the functional properties of starch straws after heating above T_g. These authors reported that lower cooling temperatures accelerated fixation of ordered molecular arrangements and increased intermolecular and intramolecular interactions between amylose and lipids/glycerine. This resulted in an increase in crystallinity with an increase in the cooling rate of starch melts. This suggests that changing the cooling rate after heating the ALC nanomaterials above T_g during IR-HMT may change the crystal structure, crystallinity, and thus functional properties of the resulting ALC nanomaterials.

HMT and recently IR-HMT have been widely used to modify starch properties. However, the authors are unaware of the use of these techniques to modify the properties of ALC nanomaterials. Therefore, the aim of this study is to investigate the effect of repeated IR-HMT followed by different cooling systems as a facile physical method to modify the properties of ALC nanomaterials, for potential use as a nanofiller in nanocomposites and as a clean label food ingredient. It is hypothesized that IR-HMT followed by different cooling systems will lead to ALC nanomaterials with stronger interactions between amylose and stearic acid, higher thermal properties and crystallinity.

2 | Experimental Section

2.1 | Materials

Commercial white normal maize starch was obtained from Tongaat Hulett (Edenvale, South Africa). Stearic acid was obtained from Sigma–Aldrich (St. Louis, USA). The moisture, ash, crude fat, and protein contents of maize starch were 9%, 0.1%, 0.2%, and 0.6%, respectively. The amylose content if maize starch was determined according to the method by megazyme (Bray, Ireland) amylose/amylopectin assay kits was 28.5%. Thermally stable alpha-amylase from *Bacillus licheniformis* (EC.3.2.1.1, 3000 U/mL) was obtained from Megazyme Ltd (Bray, Ireland). All the chemicals and reagents used were of analytical grade.

2.2 | Preparation of Amylose–Lipid Complex (ALC) Nanomaterials

The ALC nanomaterials were prepared according to the method described by Cuthbert et al. [3]. Firstly, stearic acid (1.5% w/w) (stearic acid/starch) was incorporated into maize starch according to the method described by D'Silva et al. [18]. The starch (20% w/v) containing stearic acid was then mixed with water and pasted using the IKA LR 1000 control reactor (Staufen, Germany) at 90°C, 150 rpm for 130 min. The paste was cooled to 75°C, to which thermostable α-amylase from *B. licheniformis* (EC.3.2.1.1) was added to the paste to hydrolyze the "uncomplexed" amylose and amylopectin for 10 min as described by Wokadala et al. [19]. It has been shown previously that ALCs are resistant to hydrolytic degradation by α-amylase [19]. Therefore, α-amylase is expected to hydrolyze amylopectin and uncomplexed amylose, as complexed components of starch are resistant to hydrolysis by α-amylase. The hydrolyzed paste was washed with excess distilled water about 10 times to remove the hydrolyzed materials, and the unhydrolyzed residues (ALC) were freeze dried. The residue yield (ALC) was reported to be about 30% after hydrolysis with α-amylase, which was close to the amylose content (29%) of maize starch [3].

2.3 | Infrared Heat Moisture Treatment With Different Cooling Systems

For IR-HMT, the prepared material was mixed with water to a moisture content of about 25%. The conditioned samples were then equilibrated for 24 h by sealing in the container (21°C) before HMT. Approximately 30 g of the samples were weighed

TABLE 1 | Infrared heat moisture treatment condition followed by different cooling systems.

Sample code	Infrared heat moisture treatment (110°C)	Cooling system	Total IR-HMT exposure time (h)
HH0	**No IR-HMT**	**Room temperature cooling at 23°C**	**0**
HH1	**IR-HMT for 1 continuously**		**1**
HH2	**IR-HMT for 2 continuously**		**2**
HH3	**IR-HMT for 2 continuously**		**3**
HR0	No IR-HMT	Room temperature cooling at 23°C	0
HR1	IR-HMT for 1 h followed by cooling at 23°C for 24 h (Day 1)		1
HR2	Repeated IR-HMT for 1 h followed by cooling at 23°C for 24 h (Day 2)		2
HR3	Repeated IR-HMT for 1 h followed by cooling at 23°C for 24 h (Day 3)		3
HF0	**No IR-HMT**	**Cooling using refrigeration at 4°C**	**0**
HF1	**IR-HMT for 1 h followed by cooling at 4°C for 24 h (Day 1)**		**1**
HF2	**Repeated IR-HMT for 1 h followed by cooling at 4°C for 24 h (Day 2)**		**2**
HF3	**Repeated IR-HMT for 1 h followed by cooling at 4°C for 24 h (Day 3)**		**3**
HN0	No IR-HMT	Rapid cooling with liquid nitrogen for 10 min followed by storage at −20°C	0
HN1	IR-HMT for 1 h followed by rapid cooling with liquid nitrogen for 10 min and stored at −20°C for 24 h (Day 1)		1
HN2	Repeated IR-HMT for 1 h followed by rapid cooling with liquid nitrogen for 10 min and stored at −20°C for 24 h (Day 2)		2
HN3	Repeated IR-HMT for 1 h followed by rapid cooling with liquid nitrogen for 10 min and stored at −20°C for 24 h (Day 3)		3

Note: HH means continuous infrared heat moisture treatment. HR means IR-HMT followed by cooling at room temperature. HF means IR-HMT followed by cooling in a refrigerator. HN means IR-HMT followed by rapid cooling using liquid nitrogen for 10 min and stored at −20°C. The number that follows HH/HR/HR/HF/HN denotes the cummulative exposure time to HMT at 110°C.

into glass petri dishes to a thickness of about 3 mm. IR-HMT was applied using a Microwave/Infrared Hot air tunnel oven (MW 180, Olifantsfontein, South Africa). The samples were placed at a height 25 cm away from the IR halogen lamp (0.2–4 μm) in the infrared oven. The surface temperature of the samples was measured using an IR thermometer, and the surface temperature was determined to be about 110°C.

The isolated ALC samples were IR-HMT, then cooled using different cooling systems according to Table 1. Room temperature cooling denotes slow cooling, while liquid nitrogen cooling denotes rapid cooling, with refrigeration cooling being an intermediate between the two. All the IR-HMT samples followed by different cooling samples were dried at 40°C to about 10% moisture content and stored in airtight containers at 4°C before analysis.

2.4 | Analysis

2.4.1 | Differential Scanning Calorimetry (DSC)

The thermal properties of isolated infrared heat moisture-treated ALCs samples were measured using a Mettler HP DSC827e (Greifensee, Switzerland) according to the method described by Wokadala et al. [19]. About 10 mg samples were weighed into an aluminum pan and thoroughly mixed with distilled water at a 1:3 starch to water ratio (w/w) to make a homogeneous slurry, and the pans were sealed with an aluminum lead. The pans were equilibrated for 24 h at room temperature before scanning. The samples were heated from 25 to 180°C under high pressure (4 MPa using N_2) at a heating rate of 10°C/min. An empty pan was used as a reference, and the instrument was calibrated using indium (T_p = 156.6°C, 28.45 J/g).

2.4.2 | X-Ray Diffraction (XRD)

The crystallinity of the isolated infrared heat moisture treated ALCs was analyzed using XRD X'Pert PRO diffractometer (PAN analytical, Netherlands) producing Cu Kα radiation ($\lambda = 1.54$ nm). The samples were equilibrated for 5 days at 65% estimated relative humidity (ERH) at 25°C using a saturated sodium chloride solution. The instrument was operated at a voltage and current of 45 kV and 40 mA, respectively. The samples were scanned from 5° to 30° (2θ) with a scan step size of 0.026°/s. The relative degree of crystallinity was calculated using Origin Pro software as a percentage integrated area of crystalline peaks to the total integrated area above a straight baseline using Equation (1):

$$X_c = \frac{\text{Integrated area of crystalline peaks}}{\text{Total integrated curve area}} \times 100 \quad (1)$$

2.4.3 | Dynamic Mechanical Thermal Analysis (DMTA)

The thermomechanical properties of the isolated infrared heat moisture treated ALCs were analyzed using Perkin Elmer DMA 8000 (USA). The samples were analyzed from −100 to 200°C at a heating rate of 2°C/min operated at frequency of 1 Hz. The instrument was operated in a dynamic mode using a single cantilever geometry at a strain of 0.02%.

2.4.4 | Scanning Electron Microscope (SEM)

The morphology of the isolated infrared heat moisture treated ALCs samples was visualized using a Field Emission Scanning Electron Microscope (FESEM), ZEISS (Oberkochen, Germany). Briefly, the sample sputter coated with carbon and the samples analyzed using FESEM at an accelerating voltage of 3.0 kV.

2.4.5 | Flow Properties

The flow properties of the isolated infrared heat moisture treated ALC samples were analyzed using the rheometer (Physica MCR 101, Ostildern, Germany) in a plate-to-plate configuration, using a serrated plate with a 1 mm gap. The samples were dispersed in distilled water (10% w/v) and equilibrated at 25°C for 1 min before the start of the test. The flow curves were determined at a shear rate ranging from 0.001 to 1000 s^{-1}. To determine the clockwise hysteresis loop, the shear rate was increased at a constant rate from 0.001 to 1000 s^{-1} and then decreased again to obtain an upward and downward shear rate versus viscosity curve. The upward and downward flow curves do not follow the same path and have a loop. The area of the loop between the two curves was calculated using the RheoCompass software version 1.34.1048-release (Anton Paar, Ostfildern, Germany). The Power law model ($\sigma = K\gamma^n$) was used to describe the flow properties, where K is the consistency coefficient (Pa.s^n), γ˙ is the shear rate, and n is the flow behavior index.

2.4.6 | Water Absorption Index (WAI) and Water Solubility Index (WSI)

The WAI and WSI were measured at 50 and 95°C using a method described by Mapengo and Emmambux [20]. About 1 g samples (W_o) were heated in 10 mL distilled water at 50 and 95°C in a shaking water bath operated at 150 rpm for 30 min, while vortexing every 5 min. The dispersion was then centrifuged at 3000 × g for 15 min. The supernatant was decanted and evaporated at 100°C for 24 h in a forced draught oven, and the weight of the dissolved solid was weighed (W_d). The solid residues after centrifugation were weighed and used to calculate WAI using Equation (2) expressed as the weight of the solid residue (pellet) per gram of dry ground sample (g/g):

$$\text{WAI} = \frac{\text{CTS} - \text{CT}}{W_o} \quad (2)$$

where CTS is the weight of the centrifuge tube containing the pellet after centrifugation, CT is the weight of the empty centrifuge tube, and W_o is the dry weight of the sample.

The WSI was determined as the weight ratio of the dried supernatant to the weight of the dry sample expressed as a percentage (%) using Equation (3):

$$\text{WSI} = W_d \times \frac{100}{W_o} \quad (3)$$

where W_d is the weight of dissolved solids in the supernatant (weight of supernatant after drying) and W_o is the dry weight of the sample.

2.5 | Statistical Analysis

The statistical design of the pilot scale material was a 4 × 4 factorial design (IR-HMT for 0, 1, 2, and 3 h and cooling systems; no cooling, room temperature, refrigeration temperature, and liquid nitrogen). The experiments were done in triplicate. Multivariate analysis of variance (MANOVA) was used to determine significant differences due to the IR-HMT and cooling systems for amylose lipid complex nanomaterials. Means were compared using the Fischer's least significant difference test (LSD) at $p \leq 0.05$.

3 | Results and Discussion

3.1 | Thermal, Crystallinity, and Thermomechanical Properties of ALC Nanomaterials

DSC has been a widely used technique to identify and characterize ALCs [13, 19, 21]. The melting endotherms of untreated and infrared heat moisture-treated ALC nanomaterials are shown in Figure 1 and summarized in Table S1. The untreated ALC nanomaterials (HH0, HR0, HF0, and HN0) displayed an endothermic melting peak with an onset temperature (T_o), peak temperature (T_p), and conclusion temperature (T_c) of 97, 103, and 110°C (Table S1), respectively, typical of Type I ALC [22]. Mapengo

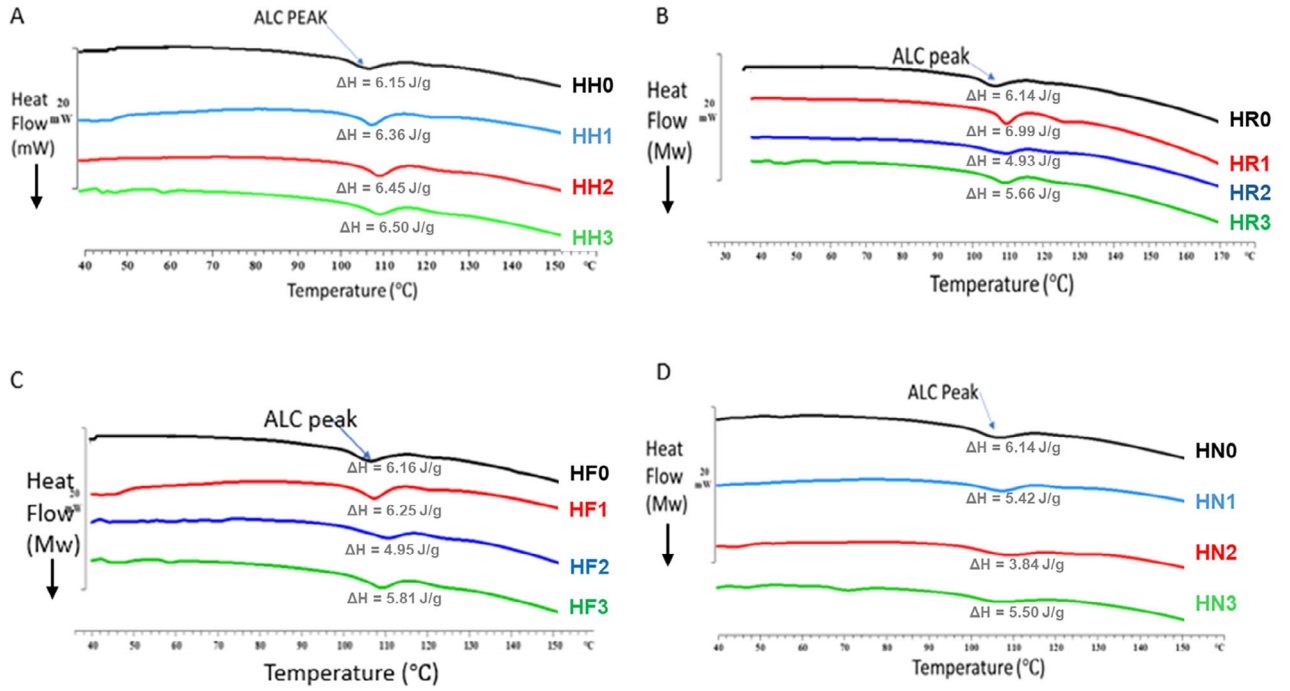

FIGURE 1 | Effect of heat moisture treatment and cooling systems on the thermal properties of isolated ALC nanomaterials. HH means continuous infrared heat moisture treatment. HR means IR-HMT followed by cooling at room temperature. HF means IR-HMT followed by cooling in a refrigerator. HN means IR-HMT followed by rapid cooling using liquid nitrogen for 10 min and stored at −20°C. The number that follows HH/HR/HR/HF/HN denotes the cummulative exposure time to HMT at 110°C. ALC, amylose–lipid complex; HMT, heat moisture treatment; IR-HMT, infrared heat moisture treatment.

et al. [13] also reported the presence of Type I ALC with similar endothermic peak for maize starch pasted with stearic acid.

The T_o, T_p, and T_c significantly increased ($p < 0.05$) with continuous IR-HMT from 1 to 3 h (Figure 1a and Table S1). Similarly, repeated IR-HMT (more energy) and the increase in the cooling rate (from room temperature to liquid nitrogen) resulted in the increase thermal stability of the ALC nanomaterials, evidenced by the significant increase ($p < 0.05$) in T_p. This suggests that repeated HMT and rapid cooling changed the crystalline order of the ALC nanomaterials. Mapengo et al. [23] also reported that IR-HMT of starch pasted with stearic acid resulted in more amylose–lipid interaction to produce more ordered crystallites and V-type crystallites.

In general, ALC can be classified according to their melting temperatures, these can be Type I (96–104°C), Type IIa (105–110°C), and Type IIb (109–120°C) [22]. Therefore, it is evident that IR-HMT and an increase in the cooling rate promoted the conversion of a less ordered crystalline structure of Type I ALC into a more ordered Type II ALC that melts at higher temperatures (Figure 1 and Table S1). Notably, IR-HMT with room temperature cooling resulted in the formation of Type IIa ALC (T_p = 109.7°C), meanwhile an increase in the cooling rate with refrigeration and liquid nitrogen resulted in more stable Type IIb ALC with T_p of 110 and 112°C (Table S1), respectively. Mapengo et al. [13] also reported that IR-HMT promoted the conversion of Type I ALC to more stable Type IIa and Type IIb crystallites. Type II crystallites are reported to be made up of distinct crystalline and amorphous regions, whereas Type I crystallites are randomly oriented with no distinct crystalline regions [13, 24]. Therefore, the conversion of Type I crystallites into Type II crystallites may increase the degree of crystallinity of the ALC nanomaterials and their strength, which is desired for application as reinforcing nanofillers in packaging materials.

The interactive effect of repeated IR-HMT and an increase in cooling rate may cause rearrangements of molecules during IR-HMT and cooling to result in different types of ALC. During IR-HMT, the ALC crystals may melt and recrystallize during rapid cooling to highly ordered crystal structures that melt at higher temperature. Thus, repeated IR-HMT may lead to more melting of poorly ordered crystal structures and recrystallization to highly ordered structures during cooling. Gong et al. [15] reported that repeated HMT and cooling of red adzuki bean starch without stearic acid resulted in stronger recrystallization and redistribution of water molecules during the heating process to form a more stable crystalline structure. Similarly, Su et al. [25] reported that repeated HMT of wheat starch and cooling may have resulted in the breaking of hydrogen bonds in starch, and cooling strengthened the connections between amylose and amylopectin, thus the starch recrystallized into more stable crystal structures after repeated HMT. Therefore, in this study, it also appears that repeated IR-HMT followed by cooling resulted in the conversion of Type I ALC into Type II ALC due to a melt recrystallization phenomenon during repeated IR-HMT and cooling. Furthermore, Type IIa ALC nanomaterials were converted to Type IIb with rapid cooling.

The melting enthalpy (ΔH), which corresponds to the melting of ALC nanomaterials, was calculated from the area under the melting peak, and the results are shown in Figure 1. The untreated

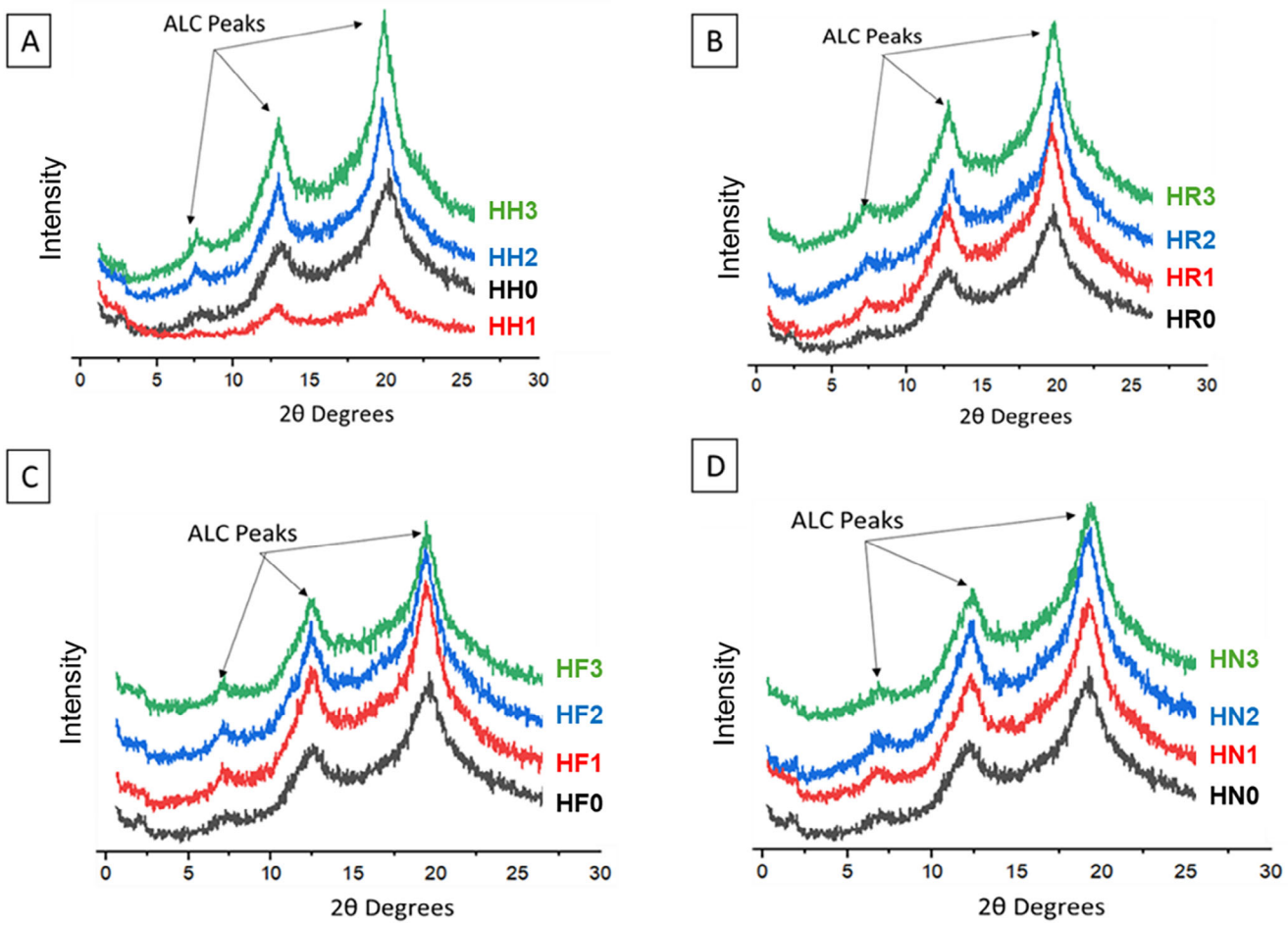

FIGURE 2 | Effect of infrared heat moisture treatment and cooling systems on the x-ray diffraction patterns of the isolated ALC nanomaterials. HH means continuous infrared heat moisture treatment. HR means IR-HMT followed by cooling at room temperature. HF means IR-HMT followed by cooling in a refrigerator. HN means IR-HMT followed by rapid cooling using liquid nitrogen for 10 min and stored at −20°C. The number that follows HH/HR/HR/HF/HN denotes the cummulative exposure time to HMT at 110°C. ALC, amylose–lipid complex; HMT, heat moisture treatment; IR-HMT, infrared heat moisture treatment.

ALC nanomaterials had an enthalpy of about 6.15 J/g. Continuous IR-HMT for 1, 2, and 3 h showed a slight increase in ΔH (Figure 1a), suggesting that more energy was used to melt the crystallites in ALC nanomaterials. However, the effect of repeated IR-HMT and different cooling systems (Figures 1b–d) did not show a clear trend on the ΔH values. The melting enthalpies may be used to indicate the degree of crystallinity, as they indicate the amount of energy used to melt the crystallites. In this case, the effect of repeated IR-HMT and different cooling systems on the degree of crystallinity is better resolved by the XRD results (Figure 2).

The crystallinity of the untreated and infrared heat moisture treated ALC nanomaterials was characterized by XRD, and the results are shown in Figure 2. The crystallinity was calculated, and the results are shown in Table S2. All the XRD diffraction patterns displayed the main diffraction peaks at 7°–8° (2θ), 12°–13° (2θ), and 19°–20° (2θ). These diffraction peaks are associated with the V-type crystallites owing to ALCs [3, 26]. Native maize starch, which was used to synthesize the ALC nanomaterials, has been characterized by A-type crystallites with diffraction peaks at 15° (2θ), 23° (2θ), and an unresolved doublet at 17° and 18° (2θ) [27, 28]. The disappearance of the peaks associated with native maize starch suggests that the crystalline structure of native maize starch was destroyed during the processing into ALC nanomaterials, and the presence of V-type crystallites suggests the successful synthesis and isolation of ALC.

The untreated ALC nanomaterials (HH0, HR0, HF0, and HN0) had a degree of crystallinity of about 14% (Table S2). The relative crystallinity of the ALC nanomaterials increased with a continuous increase in IR-HMT time from 1 to 3 h, compared to the untreated ALC nanomaterials (Table S2), except for the ALC nanomaterial IR-HMT for 1 h (Figure 2a). The relative crystallinity significantly increased ($p < 0.05$) with repeated IR-HMT (from 1 to 3 h), and the increase in the cooling rate (from room temperature to liquid nitrogen) (Figure 2). The higher relative crystallinity of the ALC nanomaterials with IR-HMT and increase in cooling rate was also supported by the increase in the endotherm melting temperatures, and the presence of Type IIa and Type IIb crystallites as previously observed from DSC. Type II crystallites have higher crystalline order compared to Type I ALC, thus require more thermal energy to melt evidenced by

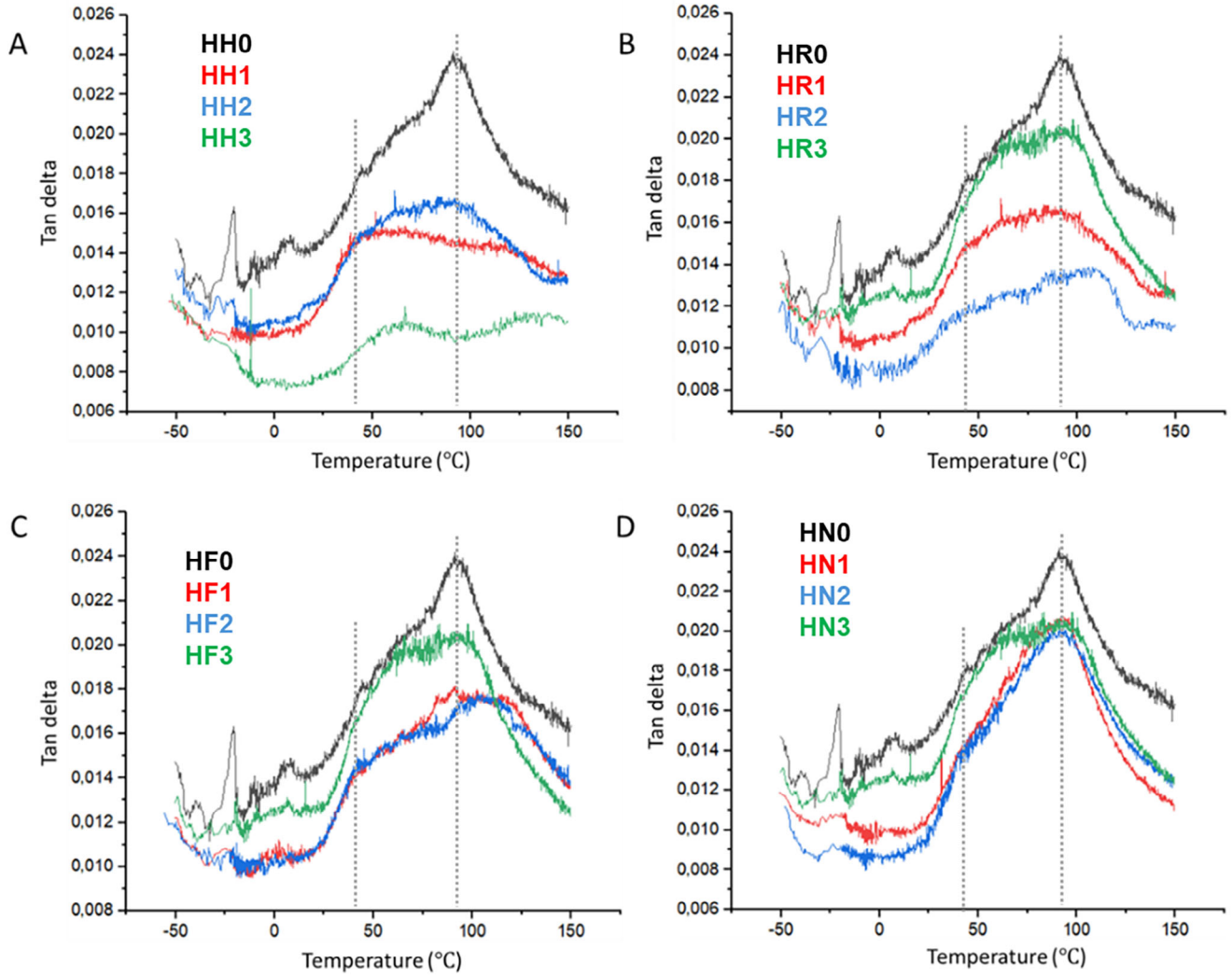

FIGURE 3 | DMTA results showing the effect of infrared heat moisture treatment and different cooling systems on the thermomechanical properties of ALC nanomaterials. HH means continuous infrared heat moisture treatment. HR means IR-HMT followed by cooling at room temperature. HF means IR-HMT followed by cooling in a refrigerator. HN means IR-HMT followed by rapid cooling using liquid nitrogen for 10 min and stored at −20°C. The number that follows HH/HR/HR/HF/HN denotes the cummulative exposure time to HMT at 110°C. ALC, amylose–lipid complex; DMTA, dynamic mechanical thermal analysis; HMT, heat moisture treatment; IR-HMT, infrared heat moisture treatment.

higher crystallinity and higher melting temperatures observed from XRD and DSC results, respectively. Mapengo et al. [13] also reported that IR-HMT resulted in higher crystallinity of IR-HMT in maize starch pasted with stearic acid due to the promotion of more ALCs and the formation of more stable Type II crystallites. Therefore, IR-HMT and faster cooling may be used to form more stable crystallites (Type II) and increase the crystallinity of ALC nanomaterials.

The thermomechanical properties of the untreated and IR-HMT ALC nanomaterials were investigated, and the results are shown in Figure 3. The untreated ALC nanomaterials displayed a shoulder peak below 50°C (indicated by dotted lines) and a main peak at a temperature between 90 and 100°C (indicated by dotted lines) (Figure 3). In general, the peak tan δ has been associated with the T_g of polymers and amorphous materials [29]. However, for starch-based materials, this concept seems to be complex. For example, Warren et al. [30] reported that for starch powders, the tan δ peak observed in DMA corresponds to the onset melting temperature observed during DSC. Thus, they attributed the tan δ peak observed during DMA to simultaneous relaxation in the amorphous region and the melting of the crystalline region that occurs during gelatinization. Therefore, for ALC nanomaterials the shoulder peak near 50°C may be associated with the relaxation of the amorphous regions of the ALC nanomaterials. Furthermore, the main tan δ peak around 90–100°C may be associated with the melting of the V-type crystallites of the ALC nanomaterials (Figure 3). This is further supported by the correspondence of the second tan δ peak to the initial melting temperature (T_o) of around 97°C as observed from DSC. The attribution of the second tan δ peak around 97–100°C to melting of V-type crystallites instead of glass transition agrees with the findings reported elsewhere [23].

The effect of IR-HMT and cooling rate on T_g of the ALC nanomaterials is difficult to ascertain conclusively. However, it is evident that the tan δ peak heights of the IR-HMT ALC nanomaterials with different cooling are lower compared to their

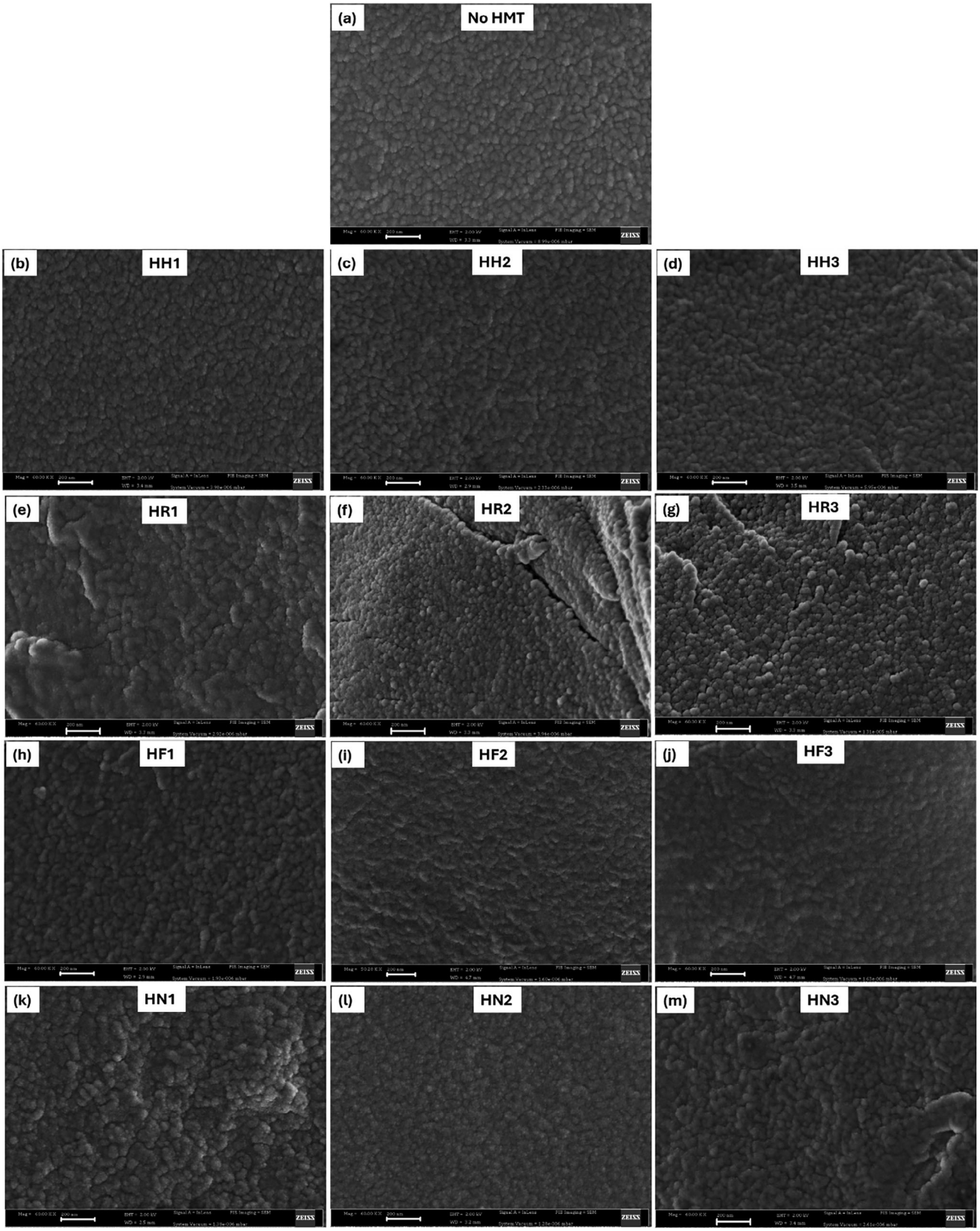

FIGURE 4 | Scanning electron microscope images of untreated and IR-HMT ALC nanomaterials. Scale bar = 200 nm (60 KX magnification). HH means continuous infrared heat moisture treatment. HR means IR-HMT followed by cooling at room temperature. HF means IR-HMT followed by cooling in a refrigerator. HN means IR-HMT followed by rapid cooling using liquid nitrogen for 10 min and stored at −20°C. The number that follows HH/HR/HR/HF/HN denotes the cumulative exposure time to HMT at 110°C. ALC, amylose–lipid complex; HMT, heat moisture treatment; IR-HMT, infrared heat moisture treatment.

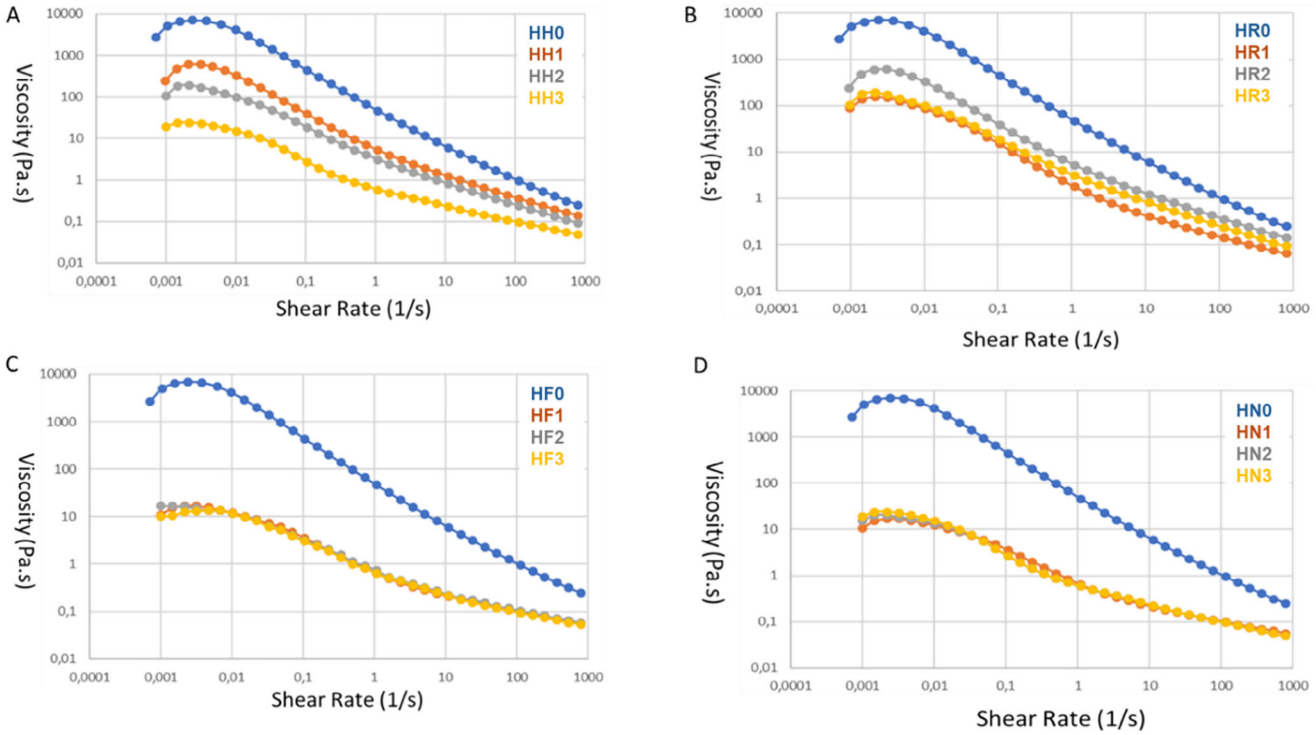

FIGURE 5 | Effect of IR HMT and cooling systems on the flow properties of isolated ALC nanomaterials. HH means continuous infrared heat moisture treatment. HR means IR-HMT followed by cooling at room temperature. HF means IR-HMT followed by cooling in a refrigerator. HN means IR-HMT followed by rapid cooling using liquid nitrogen for 10 min and stored at −20°C. The number that follows HH/HR/HR/HF/HN denotes the exposure time to HMT at 110°C. ALC, amylose–lipid complex; HMT, heat moisture treatment; IR-HMT, infrared heat moisture treatment.

untreated counterparts (HH0, HR0, HF0, and HN0) (Figure 3). Tan δ is a mechanical dampening factor defined as the ratio of loss and storage modulus (tan $\delta = E''/E'$). A higher tan δ peak height may indicate the tendency of the material to dissipate energy (high E''), while a lower tan δ peak heigh may indicate the tendency of the material to dissipate less energy (high E') [29]. Therefore, the lower tan δ peak heights (Figure 3) observed after IR-HMT with different cooling systems compared to their untreated counterparts could indicate their ability to dissipate store energy (higher E') and less dampening. This may be due to stronger interactions between amylose and stearic acid to form ALC and less molecular mobility in the amorphous components of the ALC nanomaterials. This can also be supported by knowledge borrowed from material science, in which less molecular mobility due to improved interactions between a polymer and a filler has led to a decrease in tan δ peak height, indicative of high elasticity [29, 31].

3.2 | Morphology

The morphology of the untreated and IR-HMT ALC nanomaterials was investigated by SEM, and the images are shown in Figure 4. The untreated ALC nanomaterial contained particles that were irregularly shaped to ovoid/round (Figure 4a). Although it was not possible to do image particle size analysis, the individual particles (irregular to round/ovoid) seem to have a particle size of less than 100 nm, thus confirming their nanometer scale range. Cuthbert et al. [3] reported that residues obtained after long pasting of maize/tef starch followed by hydrolysis with alpha amylase were ALC nanomaterials that are irregularly shaped, round/ovoid with a mean diameter of less than 10 nm based on atomic force microscopy (AFM) high-resolution transmission electron microscopy (HRTEM).

The ALC nanomaterials subject to IR-HMT continuously for 1, 2, and 3 h (Figure 4b–d) seemed to have a more uniform irregularly structured particles, similar to untreated ALC nanomaterials (Figure 4a). However, the ALC nanomaterials subject to IR-HMT for 1, 2, and 3 h followed by cooling at room temperature (Figures 4e–g) had particles with more round/ovoid morphology, rather than irregularly shaped particles observed with untreated ALC nanomaterials. This may be ascribed to slow cooling (room temperature) that allowed for slow crystallization after heating, leading to particles with round morphology. In contrast, fast cooling with refrigeration (Figures 4h–j) and with liquid nitrogen (Figures 4k–m) may have resulted in fast crystallization after heating, thus resulting in relatively more irregularly shaped particles than round/ovoid particles observed with slow cooling (room temperature).

3.3 | Flow Properties

The flow properties untreated and IR-HMT ALC nanomaterials were investigated, and the results are shown in Figure 5. The viscosity of all the ALC nanomaterials decreased with an increase in shear rate, evidence of a shear-thinning behavior (Figure 5). Regardless of the cooling system (room temperature, refrigeration, and liquid nitrogen), the IR-HMT ALC nanomaterials had

TABLE 2 | Effect of IR-HMT and cooling systems on the flow properties of ALC nanomaterials.

Sample	Time of HMT (h)	K (Pa.s^n)	n	r^2	Hysteresis (Pa/s)
HH0	0	46.5 ± 0.5^{f}	0.16 ± 0.1^{a}	0.99	$13\,796 \pm 0.5^{i}$
HH1	1	5.3 ± 0.2^{e}	0.45 ± 0.4^{b}	0.99	$33\,378 \pm 0.6^{h}$
HH2	2	3.3 ± 0.1^{d}	0.44 ± 0.1^{b}	0.99	3157 ± 0.2^{g}
HH3	3	2.3 ± 0.1^{c}	0.45 ± 0.1^{b}	0.99	2925 ± 0.9^{f}
HR0	0	46.7 ± 0.2^{f}	0.16 ± 0.1^{a}	0.99	$13\,817 \pm 0.3^{i}$
HR1	1	1.7 ± 0.1^{b}	0.44 ± 0.1^{b}	0.99	1672 ± 0.7^{c}
HR2	2	1.6 ± 0.1^{b}	0.45 ± 0.1^{b}	0.99	1845 ± 0.5^{d}
HR3	3	1.5 ± 0.1^{b}	0.45 ± 0.1^{b}	0.99	2045 ± 0.4^{e}
RF0	0	46.6 ± 0.1^{f}	0.16 ± 0.1^{a}	0.99	$13\,790 \pm 0.2^{i}$
RF1	1	0.4 ± 0.1^{a}	0.68 ± 0.1^{c}	0.99	665 ± 0.3^{b}
RF2	2	0.4 ± 0.1^{a}	0.68 ± 0.1^{c}	0.99	628 ± 0.5^{ab}
RF3	3	0.6 ± 0.1^{a}	0.62 ± 0.1^{c}	0.99	598 ± 0.6^{a}
HN0	0	46.8 ± 0.2^{f}	0.16 ± 0.1^{a}	0.99	$13\,784 \pm 0.3^{i}$
HN1	1	0.1 ± 0.1^{a}	0.83 ± 0.1^{e}	0.99	690 ± 0.4^{b}
HN2	2	0.2 ± 0.1^{a}	0.75 ± 0.1^{d}	0.99	601 ± 0.1^{a}
HN3	3	0.2 ± 0.1^{a}	0.74 ± 0.1^{d}	0.99	571 ± 0.8^{a}

Note: Means followed by standard deviation. Values with different letters in the column are significantly different $p < 0.05$. HH means continuous infrared heat moisture treatment. HR means IR-HMT followed by cooling at room temperature. HF means IR-HMT followed by cooling in a refrigerator. HN means IR-HMT followed by rapid cooling using liquid nitrogen for 10 min and stored at −20°C. The number that follows HH/HR/HR/HF/HN denotes cummulative exposure time to HMT at 110°C.

lower viscosity over the entire shear rate range compared to their untreated counterparts (HH0, HR0, HF0, and HN0) (Figure 5).

The flow properties of the untreated and IR-HMT ALC nanomaterials followed the Power law model with a correlation coefficient $r^2 \geq 0.99$, and the results are summarized in Table 2. The consistency index (k), viscosity, and hysteresis of the IR-HMT decreased significantly ($p < 0.05$) for all different cooling systems compared to their untreated counterparts (HH0, HR0, HF0, and HN0) (Table 2). The flow behavior index (n) of the IR-HMT increased significantly ($p < 0.05$) compared to their untreated counterparts (Table 2). This suggests that the IR-HMT ALC nanomaterials were less shear thinning and moving toward a Newtonian regime (toward $n = 1$). In general, shear-thinning behavior is observed due to molecular disentanglement with increasing shear rate as the molecules begin to orient in the direction of shear [32, 33]. The IR-HMT-treated ALC nanomaterials with more rapid cooling became less shear thinning and moved more toward the Newtonian regime due to less molecular disentanglement and less alignment in the shear direction. This may be due to stronger molecular interactions between amylose and stearic acid to form more stable ALC nanomaterials. This may also be correlated with the formation of more stable Type II crystals observed with IR-HMT followed by more rapid cooling as discussed earlier.

The flow behavior index suggests that there was an interactive effect between the intensity of IR-HMT (from 1 to 3 h) and faster cooling rate (room to liquid nitrogen) at $p < 0.05$. For example, ALC nanomaterials that were treated for longer time (from 1 to 3 h) and subject to a faster cooling rate (from room temperature to liquid nitrogen) displayed minimal or less shear thinning behavior as the n value from the Power law model increased toward 1 (Table 2), suggesting that IR-HMT and faster cooling resulted in ALC nanomaterials that have a more Newtonian fluid behavior, than shear thinning.

The increase in IR-HMT from 1 to 3 h significantly decreased the viscosity. Furthermore, the increase in the rate of cooling from room temperature to liquid nitrogen resulted in a significantly ($p < 0.05$) higher decrease in viscosity. Thus, it seems like the cooling system seemed to have a greater effect in decreasing the viscosity compared to IR-HMT. The lower viscosity of IR-HMT ALC nanomaterials suggests that there may have been changes, such as hydrodynamic volume of the ALC nanomaterials, as well as stronger molecular interactions between the nanomaterials. Lower viscosity suggests a lower hydrodynamic volume of the treated nanomaterials [33], this may also be correlated with lower water absorption properties in section 3.4.

The clockwise hysteresis loop of untreated isolated ALC nanomaterials is referred to as thixotropic behaviors, since the clockwise loop indicates the structural breakdown by the shear, resulting in the formation of new structure or changes in the structure [34]. IR-HMT and an increase in the cooling rate decreased the hysteresis loop, suggesting a more stable nanomaterial in term of recovery. The decrease in hysteresis may be attributed to rearrangement of amorphous region of the nanomaterial into more compact crystalline region as well as formation of cross-linkages [35]. Therefore, more energy is required for structural disintegration. The lower viscosity, less shear thinning, and the lower hysteresis suggest that there have been some molecular changes of the IR-HMT ALC nanomaterials.

TABLE 3 | Effect of IR-HMT on the water absorption and water solubility index of the ALC nanomaterials.

Sample	Time of HMT (h)	WAI at 50°C (g/g)	WAI at 95°C (g/g)	WSI at 50°C (%)	WSI at 95°C (%)
HH0	0	9.6 ± 0.6^{e}	20.3 ± 0.2^{e}	5.3 ± 0.3^{f}	9.8 ± 0.1^{efg}
HH1	1	8.3 ± 0.3^{d}	19.8 ± 0.2^{abcde}	4.3 ± 0.4^{cd}	9.5 ± 0.1^{cde}
HH2	2	8.2 ± 0.3^{d}	19.6 ± 0.1^{abcd}	$4.0 \pm 0.2b^{cd}$	9.2 ± 0.1^{bcd}
HH3	3	6.4 ± 0.3^{a}	19.15 ± 0.2^{a}	3.6 ± 0.1^{abc}	8.9 ± 0.1^{ab}
HR0	0	10.1 ± 0.1^{e}	20.2 ± 0.1^{de}	5.2 ± 0.1^{f}	9.9 ± 0.1^{efg}
HR1	1	8.3 ± 0.2^{d}	19.9 ± 0.1^{bcde}	4.5 ± 0.4^{de}	9.5 ± 0.2^{cde}
HR2	2	7.3 ± 0.3^{bc}	19.6 ± 0.1^{abcd}	4.1 ± 0.1^{bcd}	9.1 ± 0.1^{abc}
HR3	3	6.1 ± 0.1^{a}	19.5 ± 0.1^{abc}	3.9 ± 0.2^{bcd}	8.8 ± 0.1^{a}
RF0	0	10.1 ± 0.2^{e}	20.1 ± 0.1^{cde}	5.1 ± 0.2^{ef}	$9.9 \pm 0.1f^{g}$
RF1	1	7.3 ± 0.1^{bc}	19.8 ± 0.2^{bcde}	4.8 ± 0.1^{e}	9.6 ± 0.1^{def}
RF2	2	6.3 ± 0.2^{a}	19.5 ± 0.3^{ab}	4.3 ± 0.1^{cd}	9.2 ± 0.2^{bcd}
RF3	3	6.5 ± 0.1^{ab}	18.9 ± 0.1^{a}	4.0 ± 0.2^{bcd}	9.0 ± 0.1^{ab}
HN0	0	10.0 ± 0.2^{e}	20.3 ± 0.3^{e}	5.4 ± 0.3^{f}	9.9 ± 0.2^{g}
HN1	1	7.9 ± 0.1^{cd}	19.8 ± 0.2^{abcde}	4.5 ± 0.1^{de}	9.6 ± 0.1^{defg}
HN2	2	7.3 ± 0.2^{bc}	19.6 ± 0.2^{abcd}	3.4 ± 0.2^{a}	9.5 ± 0.1^{def}
HN3	3	8.3 ± 0.3^{d}	19.2 ± 0.1^{ab}	3.2 ± 0.2^{bc}	9.1 ± 0.2^{abc}

Note: Means followed by standard deviation. Values with different letters in the column are significantly different $p < 0.05$. HH means continuous infrared heat moisture treatment. HR means IR-HMT followed by cooling at room temperature. HF means IR-HMT followed by cooling in a refrigerator. HN means IR-HMT followed by rapid cooling using liquid nitrogen for 10 min and stored at −20°C. The number that follows HH/HR/HR/HF/HN denotes cummulative exposure time to HMT at 110°C.

3.4 | Water Absorption Index (WAI) and Water Solubility Index (WSI)

The WAI and WSI of the IR-HMT ALC nanomaterials were conducted at two temperatures, viz 50 and 95°C and the results are shown in Table 3. The WAI and WSI of untreated and IR-HMT ALC nanomaterials were higher at 95°C compared to 50°C. This is due to higher kinetic energy at higher temperatures, resulting in increased interactions between the water molecules and the ALC nanomaterials. All the IR-HMT ALC nanomaterials with different cooling systems had lower WAI and WSI compared to their untreated counterparts (HH0, HR0, HF0, and HN0) (Table 3). Mapengo et al. [13] also reported lower WAI and WSI for IR-HMT maize starch pasted with stearic acid. The lower WAI and WSI after IR-HMT may be related to the degree of crystallinity. As observed earlier from XRD (Figure 3), IR-HMT with different cooling systems resulted in an increase in the degree of crystallinity. It is well known that crystals are impermeable to water, and diffusion occurs through amorphous regions of polymers [36]. Thus, water absorption would occur through the amorphous regions of the ALC nanomaterials. Therefore, higher crystallinity after IR-HMT may have resulted in lower WAI and WSI. Furthermore, the lower WAI and WSI of the ALC nanomaterials may be related to the lower viscosity observed from flow properties (Table 2).

4 | Conclusion

Repeated IR-HMT and different cooling rates change the molecular structure of the ALC nanomaterials, resulting in changes in their functional properties. IR-HMT (more energy) and the increase in cooling rates result in ALC nanomaterials with improved thermal stability. Moreover, it converts less ordered Type I crystallites into more ordered Type II crystallites, as shown by DSC and XRD. The combined effect of IR-HMT with rapid cooling produces ALC nanomaterials with more Type IIb crystallite, reduces viscosity, water solubility, and absorption indices. The IR-HMT ALC nanomaterials have improved thermal stability and higher crystallinity, which is desirable for use as a nanofiller. Furthermore, these IR-HMT nanomaterials have potential application as a "clean label" food ingredient as a texture modifier in beverages owing to its reduced viscosity.

Author Contributions

Njabulo Gideon Maphumulo: conceptualization, methodology, formal analysis, investigation, software, writing – original draft. **Mondli Abednicko Masanabo**: writing – review and editing. **Suprakas Sinha Ray**: conceptualization, validation, funding acquisition, resources, supervision, writing – review and editing. **Mohammad Naushad Emmambux**: conceptualization, validation, funding acquisition, resources, supervision, writing – review and editing, project administration.

Acknowledgments

The authors would like to acknowledge the DSI/NRF Centre of Excellence in Food Security Grant ID number 91490 and University of Pretoria research support for funding. The authors would also like to acknowledge the Centre for Nanostructures and Advanced Materials (CeNAM) at the Council for Scientific and Industrial Research (CSIR) for providing the characterization facilities.

Conflicts of Interest

The authors declare no conflicts of interest.

Data Availability Statement

The data that support the findings of this study are available from the upon reasonable request.

References

1. H. Onyeaka, P. Passaretti, T. Miri, and Z. T. Al-Sharify, "The Safety of Nanomaterials in Food Production and Packaging," *Current Research in Food Science* 5 (2022): 763–774.

2. N. Baig, I. Kammakakam, and W. Falath, "Nanomaterials: A Review of Synthesis Methods, Properties, Recent Progress, and Challenges," *Advanced Materials* 2 (2021): 1821–1871.

3. W. O. Cuthbert, S. S. Ray, and M. N. Emmambux, "Isolation and Characterisation of Nanoparticles From Tef and Maize Starch Modified With Stearic Acid," *Carbohydrate Polymers* 168 (2017): 86–93.

4. A. Arocas, T. Sanz, and S. Fiszman, "Improving Effect of Xanthan and Locust Bean Gums on the Freeze-Thaw Stability of White Sauces Made With Different Native Starches," *Food Hydrocolloids* 23 (2009): 2478–2484.

5. S. S. Ray, M. N. Emmambux, and O. Wokadala, "Amylose-Lipid Complexes," U.S. Patent US 20200305455 A1 (2020) application number.

6. J.-Y. Kim and S.-T. Lim, "Preparation of Nano-Sized Starch Particles by Complex Formation With n-Butanol," *Carbohydrate Polymers* 76 (2009): 110–116.

7. R. Hoover, T. Hughes, H. Chung, and Q. Liu, "Composition, Molecular Structure, Properties, and Modification of Pulse Starches: A Review," *Food Research International* 43 (2010): 399–413.

8. K. Schafranski, V. C. Ito, and L. G. Lacerda, "Impacts and Potential Applications: A Review of the Modification of Starches by Heat-Moisture Treatment (HMT)," *Food Hydrocolloids* 117 (2021): 106690.

9. E. da Rosa Zavareze and A. R. G. Dias, "Impact of Heat-Moisture Treatment and Annealing in Starches: A Review," *Carbohydrate Polymers* 83 (2011): 317–328.

10. N. Ji, X. Li, C. Qiu, G. Li, Q. Sun, and L. Xiong, "Effects of Heat Moisture Treatment on the Physicochemical Properties of Starch Nanoparticles," *Carbohydrate Polymers* 117 (2015): 605–609.

11. R. Hoover and T. Vasanthan, "Effect of Heat-Moisture Treatment on the Structure and Physicochemical Properties of Cereal, Legume, and Tuber Starches," *Carbohydrate Research* 252 (1994): 33–53.

12. C. W. Chiu and D. Solarek, "Modificaion of Starches" In Starch, (Academic Press, 2009), 629–655.

13. C. R. Mapengo, S. S. Ray, and M. N. Emmambux, "Structural and Digestibility Properties of Infrared Heat-Moisture Treated Maize Starch Complexed With Stearic Acid," *International Journal of Biological Macromolecules* 180 (2021): 559–569.

14. L. M. Fonseca, S. L. M. El Halal, A. R. G. Dias, and E. da Rosa Zavareze, "Physical Modification of Starch by Heat-Moisture Treatment and Annealing and Their Applications: A Review," *Carbohydrate Polymers* 274 (2021): 118665.

15. B. Gong, M. Xu, B. Li, et al., "Repeated Heat-Moisture Treatment Exhibits Superiorities in Modification of Structural, Physicochemical and Digestibility Properties of Red Adzuki Bean Starch Compared to Continuous Heat-Moisture Way," *Food Research International* 102 (2017): 776–784.

16. J. Zou, M. Xu, J. Tian, and B. Li, "Impact of Continuous and Repeated Dry Heating Treatments on the Physicochemical and Structural Properties of Waxy Corn Starch," *International Journal of Biological Macromolecules* 135 (2019): 379–385.

17. K. Wang, F. Zou, H. Tao, et al., "Effects of Different Rapid Cooling Temperatures and Annealing on Functional Properties of Starch Straws After Thermoplastic Extrusion," *Carbohydrate Polymers* 305 (2023): 120534.

18. T. V. D'Silva, J. R. Taylor, and M. N. Emmambux, "Enhancement of the Pasting Properties of Teff and Maize Starches Through Wet–Heat Processing With Added Stearic Acid," *Journal of Cereal Science* 53 (2011): 192–197.

19. O. C. Wokadala, S. S. Ray, and M. N. Emmambux, "Occurrence of Amylose–Lipid Complexes in Teff and Maize Starch Biphasic Pastes," *Carbohydrate Polymers* 90 (2012): 616–622.

20. C. R. Mapengo and M. N. Emmambux, "Functional Properties of Heat-Moisture Treated Maize Meal With Added Stearic Acid by Infrared Energy," *Food Chemistry* 325 (2020): 126846.

21. C. Biliaderis, C. Page, L. Slade, and R. Sirett, "Thermal Behavior of Amylose-Lipid Complexes," *Carbohydrate Polymers* 5 (1985): 367–389.

22. C. G. Biliaderis and G. Galloway, "Crystallization Behavior of Amylose-V Complexes: Structure-Property Relationships," *Carbohydrate Research* 189 (1989): 31–48.

23. C. R. Mapengo, S. S. Ray, and M. N. Emmambux, "Granular Morphology, Molecular Structure and Thermal Stability of Infrared Heat-Moisture Treated Maize Starch With Added Lipids," *Food Chemistry* 382 (2022): 132342.

24. J. A. Putseys, L. Laberts, and J. A. Delcour, "Amylose-Inclusion Complexes: Formation, Identity and Physico-Chemical Properties," *Journal of Cereal Science* 51 (2010): 238–247.

25. C. Su, K. Zhao, B. Zhang, et al., "The Molecular Mechanism for Morphological, Crystal, Physicochemical and Digestible Property Modification of Wheat Starch after Repeated versus Continuous Heat-Moisture Treatment," *LWT* 129 (2020): 109399.

26. J. Brisson, H. Chanzy, and W. Winter, "The Crystal and Molecular Structure of VH Amylose by Electron Diffraction Analysis," *International Journal of Biological Macromolecules* 13 (1991): 31–39.

27. M. A. Masanabo, S. S. Ray, and M. N. Emmambux, "Properties of Thermoplastic Maize Starch-Zein Composite Films Prepared by Extrusion Process Under Alkaline Conditions," *International Journal of Biological Macromolecules* 208 (2022): 443–452.

28. R. Utrilla-Coello, C. Hernández-Jaimes, H. Carrillo-Navas, et al., "Acid Hydrolysis of Native Corn Starch: Morphology, Crystallinity, Rheological and Thermal Properties," *Carbohydrate Polymers* 103 (2014): 596–602.

29. N. Saba, M. Jawaid, O. Y. Alothman, and M. Paridah, "A review on Dynamic Mechanical Properties of Natural Fibre Reinforced Polymer Composites," *Construction & Building Materials* 106 (2016): 149–159.

30. F. J. Warren, P. G. Royall, P. J. Butterworth, and P. R. Ellis, "Immersion Mode Material Pocket Dynamic Mechanical Analysis (IMP-DMA): A Novel Tool to Study Gelatinisation of Purified Starches and Starch-Containing Plant Materials," *Carbohydrate Polymers* 90 (2012): 628–636.

31. L. A. Pothan, Z. Oommen, and S. Thomas, "Dynamic Mechanical Analysis of Banana Fiber Reinforced Polyester Composites," *Composites Science and Technology* 63 (2003): 283–293.

32. S. U. Sajjan and M. R. Rao, "Effect of Hydrocolloids on the Rheological Properties of Wheat Starch," *Carbohydrate Polymers* 7 (1987): 395–402.

33. S. M. Tosh, P. J. Wood, Q. Wang, and J. Weisz, "Structural Characteristics and Rheological Properties of Partially Hydrolyzed Oat B-Glucan: The Effects of Molecular Weight and Hydrolysis Method," *Carbohydrate Polymers* 55 (2004): 425–436.

34. P. Achayuthakan and M. Suphantharika, "Pasting and Rheological Properties of Waxy Corn Starch as Affected by Guar Gum and Xanthan Gum," *Carbohydrate Polymers* 71 (2008): 9–17.

35. M. Sharma, D. N. Yadav, A. K. Singh, and S. K. Tomar, "Rheological and Functional Properties of Heat Moisture Treated Pearl Millet Starch," *Journal of Food Science and Technology* 52 (2015): 6502–6510.

36. A. Rodriguez-Uribe, T. Wang, A. K. Pal, F. Wu, A. K. Mohanty, and M. Misra, "Injection Moldable Hybrid Sustainable Composites of BioPBS and PHBV Reinforced with Talc and Starch as Potential Alternatives to Single-Use Plastic Packaging," *Composites Part C: Open Access* 6 (2021): 100201.

Supporting Information

Additional supporting information can be found online in the Supporting Information section.

Supporting Figure 1: star70062-sup-0001-SuppMat.docx